

# Investigating dynamic mechanisms for synchronous variation of East Asian and Australian summer monsoons over the last millennium



Jian Shi <sup>a</sup>, Qing Yan <sup>b,c,\*</sup>, Huijun Wang <sup>b,c</sup>, Dabang Jiang <sup>b,c</sup>, Jinzhong Min <sup>c</sup>, Ying Jiang <sup>d</sup>

<sup>a</sup> College of Atmospheric Science, Nanjing University of Information Science and Technology, Nanjing, China

<sup>b</sup> Nansen-Zhu International Research Centre, Institute of Atmospheric Physics, Chinese Academy of Sciences, Beijing, China

<sup>c</sup> Collaborative Innovation Center on Forecast and Evaluation of Meteorological Disasters, Nanjing University of Information Science and Technology, Nanjing 210044, China

<sup>d</sup> Shaoxing Meteorological Office, Shaoxing, China

## ARTICLE INFO

### Article history:

Received 9 December 2016

Received in revised form 5 May 2017

Accepted 11 May 2017

Available online 13 May 2017

### Keywords:

Multi-model ensemble

Symmetrical change

Total solar irradiation

Tropical temperature gradient

## ABSTRACT

The investigation into the past behavior of the East Asian summer monsoon (EASM) and Australian summer monsoon (ASM) is potentially helpful for advancing our knowledge of projected future changes. Geological evidence supports an in-phase change of the two monsoon systems over the last millennium, but the dynamic mechanisms and timescale-dependence are not fully understood. Using model outputs from the Paleoclimate Modelling Intercomparison Project Phase III, we investigated EASM and ASM variations, their phase relationship during the last millennium, and their dynamic mechanisms. According to selected “best-performance” models capable of reproducing reconstructed Asian–Australian monsoon changes, EASM and ASM showed significant in-phase changes only on centennial timescales, with intensified EASM/ASM during the Medieval Climate Anomaly (MCA) and weakened monsoons during the Little Ice Age (LIA). Moreover, the synchronous variation was more robust during the LIA relative to the MCA. The strengthened (weakened) EASM during the MCA (LIA) is attributed to an enhanced (reduced) land–sea temperature contrast and a northward (southward) shift of the subtropical westerly jet stream during boreal summer. During the same period, the ASM was reinforced (suppressed) due to the enhanced (reduced) lower-level easterly from the western Pacific and southward (northward) shift of upper-level westerly during austral summer. Meanwhile, the stronger (weaker) EASM/ASM during the MCA (LIA) was associated with expansion (retreat) of the local Intertropical Convergence Zone and an enhanced (reduced) zonal temperature gradient over the equatorial Pacific. Our results imply that the synchronous change in the Asian–Australian monsoon may be caused by inherent solar variations, further strengthening previous findings.

© 2017 Elsevier B.V. All rights reserved.

## 1. Introduction

The Asian–Australian monsoon is one of the most important components of the global monsoon system. It includes two sub-monsoon systems around the western Pacific: the East Asian monsoon and Australian monsoon, which exert great impacts on Asian and Australian hydrological changes in local summer. When the Australian summer monsoon (ASM) strengthens, precipitation is expected to increase over northern Australia (e.g., Nicholls et al., 1982; Kajikawa et al., 2010), namely, the Australian monsoon region. As the East Asian summer monsoon (EASM) gets stronger, precipitation is generally enhanced over North China and reduced over South China or the Yangtze River valley (e.g., Tao, 1987; Ding et al., 2008). Additionally,

the two monsoon systems interact with each other via cross-equatorial flows in both the lower and upper troposphere (e.g., He et al., 2007); the El Niño–Southern Oscillation modulates their interactions primarily on interannual timescales (e.g., Meehl and Arblaster, 1998; Lau and Nath, 2000).

Observational-based studies indicate that the EASM experienced a weakening trend during the last half century (e.g., Jiang and Wang, 2005; Song et al., 2014; Zhang and Zhou, 2015), and the ASM and associated rainfall was enhanced slightly over the last half century, especially since the 1980s (Li et al., 2013; Zhang and Moise, 2016). These results indicate that EASM and ASM variations are broadly anti-phase on decadal timescales. However, due to the relatively short time span of modern observations, it is unclear how the EASM and ASM behaved in the past and whether their relationship varies on different timescales.

Geological evidence helps extend monsoon records to several millennia and even longer. On millennial timescales, the EASM and ASM generally show an anti-phase variation. Proxies reveal that the EASM weakened during the whole Holocene (from ~9 kyr BP) (e.g.,

\* Corresponding author at: Nansen-Zhu International Research Centre, Institute of Atmospheric Physics, Chinese Academy of Sciences, 40 Huayuanli, Chaoyang District, Beijing 100029, China.

E-mail address: [yanqing@mail.iap.ac.cn](mailto:yanqing@mail.iap.ac.cn) (Q. Yan).

Wang et al., 2005a, 2005b; Hu et al., 2008). In contrast, several ASM records consistently show an increasing ASM trend from the early Holocene (e.g., Partin et al., 2007; Griffiths et al., 2009). Eroglu et al. (2016) also suggested a see-saw relationship between the Asian–Australian summer monsoon since the Holocene. On centennial timescales, Zhang et al. (2008) indicated an intensified Asian summer monsoon during the Medieval Climate Anomaly (MCA) and a reduced EASM during the Little Ice Age (LIA) based on  $\delta^{18}\text{O}$  records from cave speleothems. This result has been confirmed by other cave speleothems  $\delta^{18}\text{O}$  records as well as through reconstructed precipitation patterns (e.g., Tan, 2007; Chen et al., 2015). Multi-proxies in northern Australia suggest that the ASM region was generally wetter (drier) during the MCA (LIA) (e.g., Burrows et al., 2014; Denniston et al., 2015, 2016; Rouillard et al., 2016). By combining paleo-hydrology records over EASM and ASM regions, Yan et al. (2015) suggested that there was a synchronously weakened EASM and ASM during the LIA. The proposed synchronous change is distinct from the anti-phase monsoon variations in different hemispheres on a millennial timescale. Given the sporadic proxies and limited environmental variables derived from those proxies, dynamic mechanisms driving EASM–ASM variations are not fully understood.

Numerical modeling allows us to investigate possible mechanisms of monsoon changes revealed by reconstructions. It has been widely acknowledged that the out-of-phase variation of the EASM and ASM on millennial timescales (i.e., from early to middle Holocene) was induced by the northward shift of the Intertropical Convergence Zone (ITCZ) due to a precession cycle (e.g., Wyrwoll et al., 2007; Kutzbach et al., 2008; Mohtadi et al., 2016). On centennial timescales (i.e., last millennium), their relationship and dynamic mechanisms have not yet been thoroughly studied. Most research concerning the EASM suggested that solar irradiation and volcanic eruptions are primary drivers for strengthened (weakened) EASM in the MCA (LIA) (e.g., Liu et al., 2011; Man et al., 2012). However, ASM variations and their relationship with EASM over the last millennium have received little attention. Recently, Yan et al. (2015) interpreted the synchronous weakening of the EASM and ASM during the LIA as the contraction of ITCZ over that period caused by lower total solar irradiation (TSI). However, proposed mechanisms were concluded from a single model and mainly focused on the LIA. Is this hypothesis model-dependent and time interval-selected, or do other factors play a role? These issues require further examination with multiple climate models.

The Paleoclimate Modelling Intercomparison Project (PMIP) provides a platform to explore possible dynamic mechanisms behind past climate change (e.g., Braconnot et al., 2012; Bothe et al., 2013; Shi et al., 2016). In this study, we investigated EASM and ASM variations

based on PMIP3 simulations of the last millennium and focused on their phase relationship. Understanding these issues will deepen our knowledge of global monsoon variations and monsoon interactions between two hemispheres, further promoting our understanding of modern climate change. The remainder of this paper is organized as follows: in Section 2, we briefly introduce the PMIP3 models and methods used in this study. In Section 3, the PMIP3 model performance is evaluated in reproducing observed precipitation climatology and reconstructed EASM and ASM changes. In Section 4, we present the temporal evolution of the EASM and ASM and possible dynamic mechanisms. We discuss and summarize our results in Sections 5 and 6, respectively.

## 2. Data and methods

The simulations for the last millennium were obtained from nine climate models in the PMIP3, excluding MIROC-ESM because of its climate drift in long-term experiments (Sen Gupta et al., 2013). These simulations roughly span 850–1850 CE, forced by TSI, volcanic eruptions, orbital parameters, land cover and greenhouse gases. Information summarizing these PMIP3 models is given in Table 1, and details are available online at <https://pmip3.lscce.ipsl.fr/>. Modeled monthly outputs of precipitation, air temperature, sea level pressure, wind fields, outgoing longwave radiation (OLR) and sea surface temperature (SST) were used for analysis. The MCA was selected as 950–1250 CE and the LIA as 1500–1800 CE, with an identical time interval as the MCA. Model outputs and observations were interpolated to a mid-range horizontal grid resolution of  $2.0^\circ \times 2.0^\circ$  by a bilinear interpolation before performing the model–observation comparison and calculating the multi-model ensemble mean (MEM).

Because long-term monsoon variations were usually derived from precipitation-relevant proxies (e.g., Zhang et al., 2008; Denniston et al., 2016), we define regionally averaged local summer precipitation in North China ( $100^\circ\text{--}120^\circ\text{E}$ ,  $35^\circ\text{--}45^\circ\text{N}$ ) and the northern edge of Australia ( $120^\circ\text{--}150^\circ\text{E}$ ,  $10^\circ\text{--}20^\circ\text{S}$ ) as the EASM and ASM intensity over the last millennium, respectively. Local summer represents June–July–August for the EASM and December–January–February for the ASM.

## 3. Model evaluation

We first used the Taylor diagram (Taylor, 2001) to evaluate the performance of nine PMIP3 models in simulating present-day precipitation over the East Asia–western Pacific–Australia region ( $90^\circ\text{--}160^\circ\text{E}$ ,  $30^\circ\text{S--}60^\circ\text{N}$ ) (Fig. 1). The result shows that the PMIP3 models have acceptable performance in reproducing observed annual and seasonal precipitation over this region, although the accuracy of individual models varied.

**Table 1**  
PMIP3 model simulations information and their main forcings.

Model	Model full name	Resolution		Forcing	
		Atmosphere	Ocean	Solar	Volcanic
BCC-CSM-1.1	Beijing Climate Center Climate System Model (version 1.1)	128 × 64, L26	360 × 232, L40	Vieira et al. (2011), Wang et al. (2005a, 2005b)	Gao et al. (2008)
CCSM4	Community Climate System Model (version 4.0)	288 × 192, L26	320 × 384, L60	Vieira et al. (2011)	Gao et al. (2008)
CSIRO-Mk3L-1.2	Commonwealth Scientific and Industrial Research Organization (Mark 3 Low-resolution model version 1.2)	64 × 56, L18	128 × 112, L21	Steinilber et al. (2009)	Crowley et al. (2008)
FGOALS-s2	Flexible Global Ocean–Atmosphere–Land System Model (Spectral Version 2)	128 × 60, L26	360 × 180, L30	Vieira et al. (2011), Wang et al. (2005a, 2005b)	Gao et al. (2008)
GISS-E2-R	E2 version of the Goddard Institute for Space Studies Climate Model (Model E/Russell)	144 × 90, L40	288 × 180, L32	Vieira et al. (2011) Wang et al. (2005a, 2005b)	Gao et al. (2008)
HadCM3	Hadley Climate Model (version 3)	96 × 73, L19	288 × 144, L20	Steinilber et al. (2009), Wang et al. (2005a, 2005b)	Crowley et al. (2008)
IPSL-CM5A-LR	Earth System Model of the Institut Pierre Simon Laplace (low resolution)	96 × 95, L39	182 × 149, L31	Vieira et al. (2011), Wang et al. (2005a, 2005b)	Gao et al. (2008)
MPI-ESM-P	Earth System Model of Max-Planck-Institut für Meteorologie (low resolution grid and paleo mode)	196 × 98, L47	256 × 220, L40	Vieira et al. (2011), Wang et al. (2005a, 2005b)	Crowley et al. (2008)
MRI-CGCM3	Meteorological Research Institute Coupled ocean–atmosphere General Circulation Model (version 3)	320 × 160, L48	364 × 368, L51	Delaygue and Bard (2009), Wang et al. (2005a, 2005b)	Gao et al. (2008)

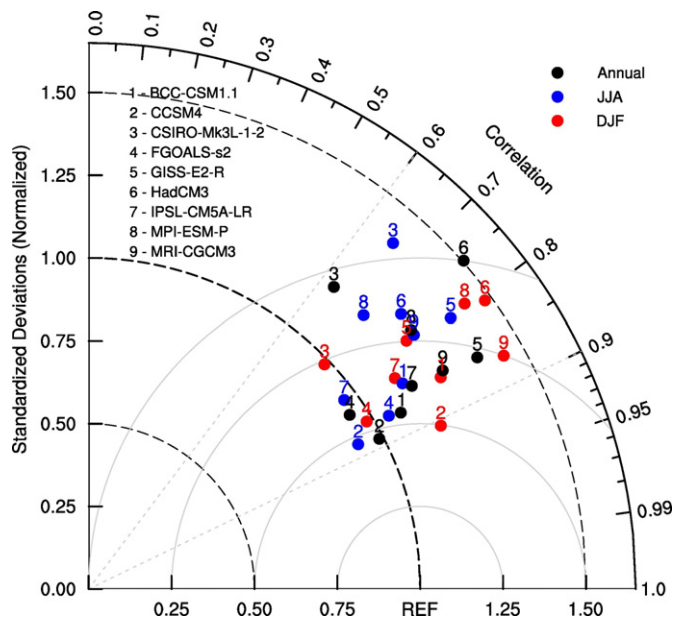


**Fig. 1.** Taylor diagram displaying pattern statistics of climatological annual and local summer precipitation over Asia-western Pacific-Australia region (30°S–60°N, 90°–160°E) between the historical experiments and observation. The radial coordinate is the standard deviation normalized by the observation, and the angular coordinate is the correlation with observation. The normalized CRMSE between a model and observation (marked as REF) is their distance apart. Note that pre-industrial experiment of CSIRO-Mk3L-1-2 is calculated due to its lack of historical experiments. The Global Precipitation Climatology Project monthly precipitation dataset V2.2 is taken as the target observed precipitation (Adler et al., 2003).

Spatial correlation coefficients between simulations and observation ranged from 0.62 to 0.88, 0.66 to 0.87 and 0.72 to 0.91 for annual, boreal summer and austral summer precipitation, respectively. All correlation coefficients pass the 99% significance test. The corresponding centered root-mean-square errors ranged from 0.48 to 1.00, 0.49 to 1.04 and 0.50 to 0.81. In general, the nine PMIP3 models reliably reproduced the spatial pattern and precipitation magnitude over the East Asia–Australia region, with better performance in simulating austral summer precipitation, providing confidence for applying them to study EASM and ASM changes during the last millennium.

Nevertheless, PMIP3 models varied widely in reproducing reconstructed EASM and ASM anomalies between the MCA and LIA (Fig. 2). Seven out of nine models (excepting BCC-CSM1-1 and FGOALS-s2) indicated sufficient precipitation over North China during the MCA relative to the LIA, which is roughly consistent with geological evidence (e.g., Tan, 2007; Chen et al., 2015). Five out of the nine models (i.e., CSIRO-Mk3L-1-2, GISS-E2-R, IPSL-CM5A-LR, MPI-ESM-P, and MRI-CGCM3) broadly simulate increased precipitation in northern Australia during the MCA, in agreement with the humidity records over that region (e.g., Zhang et al., 2008; Denniston et al., 2016). However, the remaining models indicated dry conditions or slight changes in precipitation.

To quantitatively examine precipitation variations over the two monsoon regions, Fig. 3 shows the regionally averaged EASM and ASM precipitation anomaly (i.e., the monsoon intensity change) between the MCA and LIA. The PMIP3 models show a better consistency in simulating the reconstructed EASM than the ASM during the past millennium: seven (five) out of nine models indicated a stronger EASM (ASM) during the MCA relative to the LIA. Overall, five out of the nine PMIP3 models (i.e., CSIRO-Mk3L-1-2, GISS-E2-R, IPSL-CM5A-LR, MPI-ESM-P, and MRI-CGCM3) captured the in-phase relationship between the EASM and ASM suggested by multiple proxies (Yan et al., 2015). Therefore, we used the MEM of these five models to further explore the possible mechanisms responsible for EASM and ASM variation during the last millennium.

## 4. Results

### 4.1. The relationship between EASM and ASM during the last millennium

Although reconstructions have suggested a strengthened (weakened) EASM and ASM during the MCA (LIA), it remains unclear over what timescale they were in-phase due to the coarse time resolution of proxies. To find their phase relationship on different timescales, a moving average with a variable window size was calculated. Fig. 4 shows the correlation coefficient between the EASM and ASM increased with a larger window length but decreased once the window size exceeded ~130 a. Notably, their positive relationship was only significant when the window size ranged from ~40 a to ~110 a (Fig. 4B), which indicates that the in-phase exhibition of the EASM and ASM mainly occurred on centennial timescales during the last millennium.

Fig. 5 shows the 71-a moving average of the EASM and ASM as their positive correlation is relatively more significant in this moving window width. The simulated EASM and ASM were broadly synchronous during the last millennium, consistent with reconstructions (e.g., Zhang et al., 2008; Denniston et al., 2016); their in-phase relationship was more significant during the LIA than the MCA. During the MCA, the EASM and ASM were not exactly in-phase and were even out-of-phase around 1100 CE, primarily due to a weaker ASM at that time—a cause also indicated by several proxy records. For instance, a stalagmite record in northwestern Australia suggested that the ASM was relatively weak around 1100 CE in contrast to its overall strengthening during the MCA (Denniston et al., 2016). Generally, the MEM simulation exhibits enhanced (suppressed) EASM and ASM during the MCA (LIA), which is also suggested by proxies, making it reasonable to investigate dynamic mechanisms driving the reconstructions.

### 4.2. Possible dynamic mechanisms

In this subsection, we investigate anomalous monsoon circulation and associated dynamic mechanisms. The EASM increased in the MCA relative to the climatological mean, illustrated by anomalous southwesterly winds in the subtropical regions and southeasterly winds in the extratropical East Asian regions in the lower troposphere (i.e., 850 hPa) (Fig. 6A).

The tropospheric mean temperature over the Asian continent rose faster than the mean temperature of the tropical ocean due to a different thermal capacity between land and ocean, forming an anomalous low-pressure system over the Asian continent (Fig. 7A). Thus, the meridional land–sea pressure gradient increased, which strengthened southerly winds from tropical oceans. Similarly, the temperature gradient between the Asian continent and mid-latitude North Pacific was also amplified, resulting in an enhanced zonal land–sea pressure contrast, strengthening southeasterly winds from the North Pacific. During the LIA, the mean tropospheric temperature decreased over the Asian continent and increased over adjacent oceans (Fig. 7B), causing a reduced land–sea thermal gradient, which weakened the EASM (Fig. 6B).

In the upper troposphere (i.e., 200 hPa), the East Asian subtropical westerly jet is an important component of the EASM system (Tao, 1987) and is closely associated with lower-level circulation and precipitation over the EASM region (Zhang et al., 2006). Although zonal wind was broadly weakened (strengthened) during the MCA (LIA) over the mid-latitude Asian region, the magnitude of the wind anomaly was larger south of its jet axis (approximately 37°N) than north (Fig. 8A and B). This result corresponds to a northward (southward) shift of the East Asian subtropical westerly jet and was favorable (unfavorable) for a northward rain belt shift in East Asia and a stronger EASM (e.g., Zhou and Yu, 2005).

The ASM was strengthened during the MCA and characterized by anomalous northeasterly winds from the tropical western Pacific (Fig. 6C), induced by a stronger warming over the western Pacific than the central eastern Pacific (Fig. 7C). During the LIA, the decreased ASM

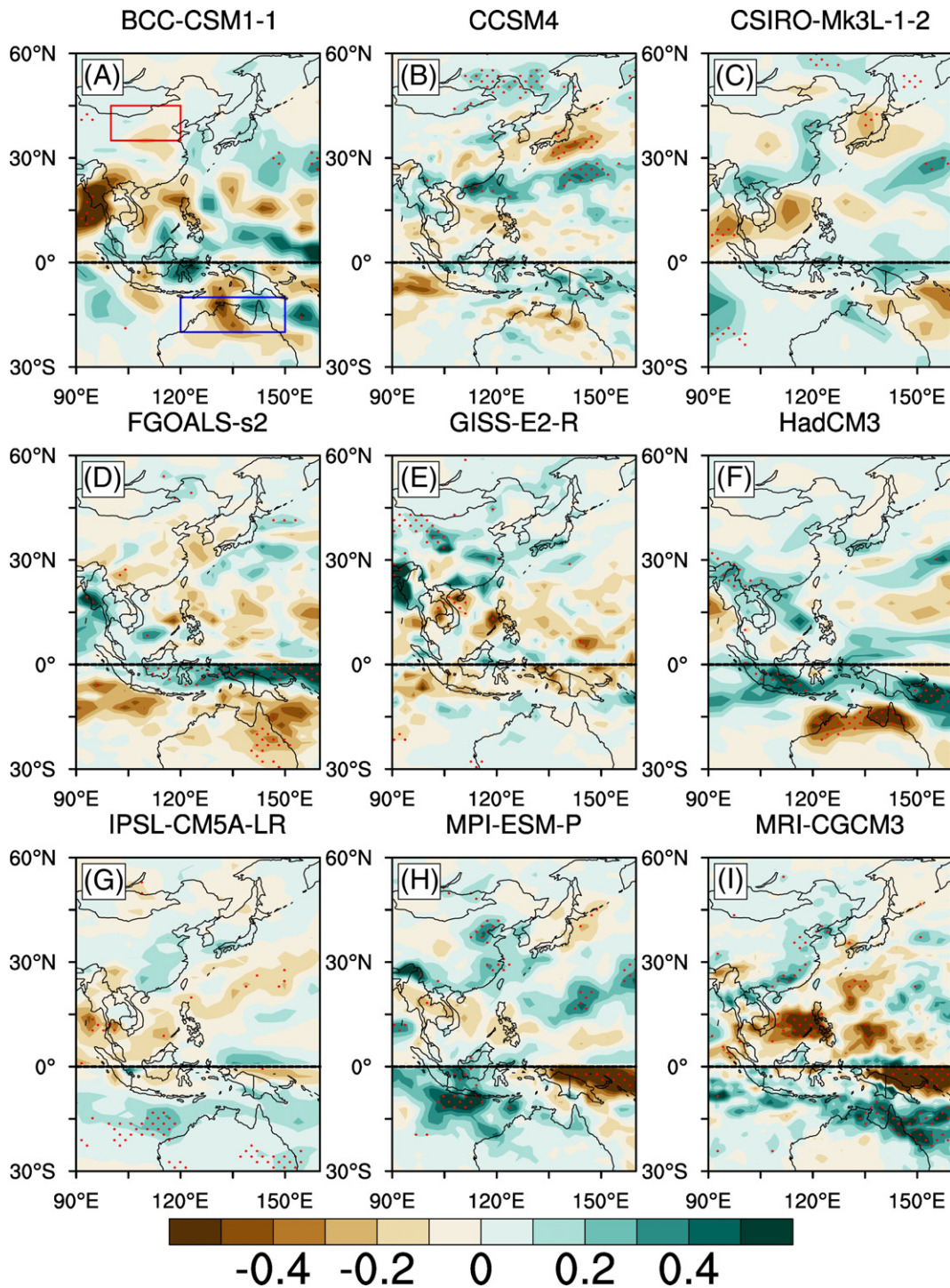


**Fig. 2.** Local summer precipitation differences between the MCA and LIA (units: mm/d). Values with  $\geq 95\%$  confidence level are dotted in red according to Student's *t*-test. Two regions used for calculating the EASM and ASM intensity are marked by rectangles in (A): North China ( $105^{\circ}\text{--}120^{\circ}\text{E}$ ,  $35^{\circ}\text{--}45^{\circ}\text{N}$ ) and northern Australia ( $120^{\circ}\text{--}150^{\circ}\text{E}$ ,  $10^{\circ}\text{--}20^{\circ}\text{S}$ ). Dash lines represent the equator.

consisted of two branches of anomalous southerlies from the tropical Indian Ocean and the tropical western Pacific Ocean (Fig. 6D). The western branch of the weakened ASM from the Indian Ocean originated from an anomalous anticyclone in the subtropical South Indian Ocean, caused by the anomalous cooling center (Fig. 7D). The eastern branch was induced by an anomalous cyclone northwest of Australia that weakened the lower-level Walker circulation (Fig. 6D), consistent with a depressed temperature gradient between the tropical western Pacific and central eastern Pacific Ocean (Fig. 7D). Notably, the magnitude of the ASM anomaly in the MCA was slightly smaller relative to the LIA.

This is attributed to different zonal locations of the anomalous cyclone/anticyclone in the South Indian Ocean, which resulted in tropical wind in the Indian and Pacific Oceans converging at approximately  $110^{\circ}\text{E}$  during the MCA but diverging at  $130^{\circ}\text{E}$  during the LIA, making ASM changes more drastic than those during the LIA.

As shown in Fig. 8C and D, the austral summer mean upper-level westerly jet was climatologically centered along  $40^{\circ}\text{S}$ . There was a weakened (strengthened) westerly north of the jet axis and a strengthened (weakened) westerly south during the MCA (LIA). This southward (northward) shift of the westerly jet is consistent with a southward

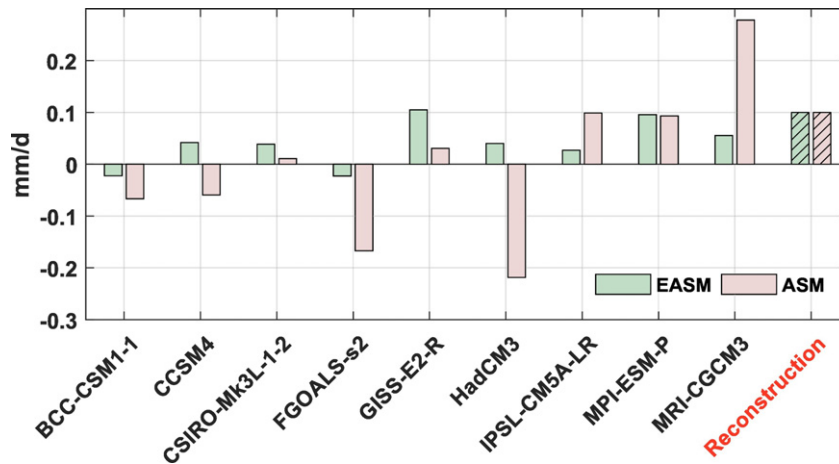


**Fig. 3.** Regionally averaged local summer precipitation differences of North China and northern Australia between the MCA and LIA. Units: mm/d. Qualitative values for reconstruction are shown in the last column.

(northward) shifted Hadley cell, conducive to an enhanced (decreased) lower-level northerly in northern Australia. In addition, there was an anomalous upper-level westerly (easterly) in the tropical western Pacific during the MCA (LIA), together with an increased (decreased) easterly at lower-level (Fig. 6C and D), implying an enhanced (weakened) Walker circulation. Together, these features led to a strengthened (weakened) ASM and ASM rainfall (Meehl and Arblaster, 1998) during the MCA (LIA).

## 5. Discussion

Synchronous variations of the EASM and ASM are a relatively robust observation among multiple model simulations (revealed by five out of nine models). During the MCA (LIA), the strengthened (weakened) EASM is attributed to enhanced (reduced) lower-level anomalous winds from tropical oceans to land and the northward (southward) shift of upper-level westerly jets at mid-latitude during boreal summer. In addition, the ASM increased (decreased) during the same period. The associated subtropical jet moved poleward (equatorward), which was symmetrical to the East Asian subtropical westerly jet shift around the equator.

The symmetrical atmospheric change in two summer hemispheres was also detected in the ITCZ. The lowest simulated tropical OLR, which represents the strongest convection, broadly reproduced the seasonal position of the ITCZ (Fig. 9). During the MCA (LIA), the boreal summer OLR decreased (increased) north of the ITCZ and increased (decreased) at the ITCZ region and further south, indicating a northward (southward) shift of the ITCZ (Fig. 9A and B). During the MCA,

relative to the LIA, the northward ITCZ corresponded to an intensified Asian summer monsoon (Fig. 6A and B). With respect to austral summer, the OLR increased over tropical western Pacific and Australia during the MCA with a larger (smaller) increase in the north (south) (Fig. 9C), resulting in a southward shift of the local ITCZ, which is consistent with an enhanced ASM (Fig. 6C). Similarly, the local ITCZ migrated northward during the LIA (Fig. 9D), in agreement with a reduced ASM, as shown in Fig. 6D. This result indicates an expansion (contraction) of the ITCZ during the MCA (LIA) on centennial timescales, which led to an in-phase change of the Asian–Australian monsoon (Yan et al., 2015).

Additionally, we found the synchronous variation of the two monsoons was also influenced by a zonal temperature gradient over tropical Pacific region. During the MCA (LIA), the zonal SST gradient (Fig. 10C) was enhanced (reduced), which led to a strengthened (weakened) Walker circulation, and hence, a stronger (weaker) EASM and ASM (e.g., Huang and Wu, 1989; Meehl and Arblaster, 1998). The strengthened (weakened) zonal SST gradient is consistent with the La Niña- (El Niño-) like conditions according to proxies from the MCA (LIA) (e.g., Cobb et al., 2003; Mann et al., 2008; Conroy et al., 2009), although uncertainties exist (e.g., Yan et al., 2011; Rustic et al., 2015).

Summertime ITCZ migration and monsoon variation were affected by inter-hemispheric insolation gradients (e.g., An et al., 2015). Fig. 10 shows that the EASM and ASM variations generally agreed with changes in TSI, although phase differences exist. Meanwhile, expanded (retreated) ITCZ occurred during the MCA (LIA) with higher (lower) TSI (Fig. 9) as well as an enhanced (reduced) zonal SST gradient over the tropical Pacific (Fig. 10). These results imply that synchronous monsoon variations may be controlled by inherent solar variations during

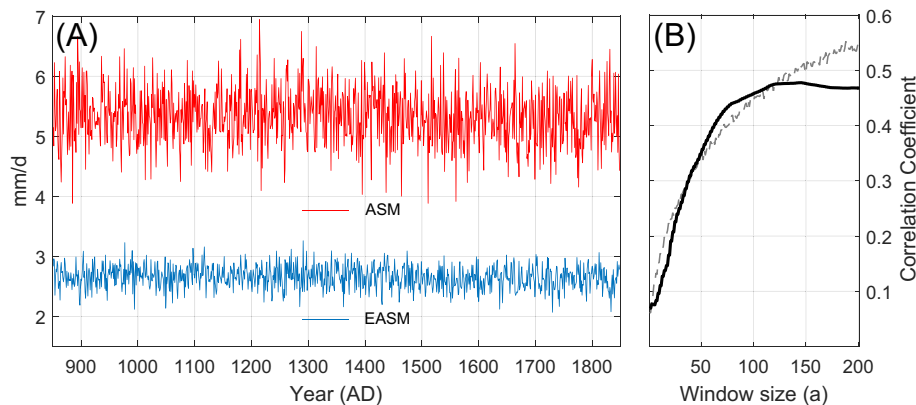


**Fig. 4.** (A) Local summer precipitation (units: mm/d) representing the EASM and ASM intensity during the past millennium based on the MEM simulation and (B) their correlation coefficient according to different width of moving average window (solid line) and the dash line represent the 95% confidence level tested by 10,000 Monte Carlo simulations.

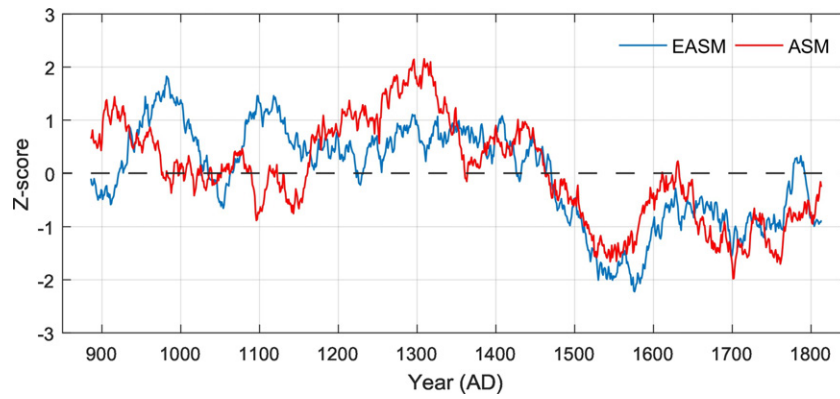


Fig. 5. Standard EASM and ASM intensity smoothed by 71-a moving average.

the past millennium, in agreement with the findings of Yan et al. (2015). This hypothesis is also supported by previous modeling studies. Liu et al. (2009) found that monsoon precipitation in both hemispheres increased (decreased) during the MCA (LIA) based on the ECHO-G simulation, which was in phase with changes in solar irradiation. Yan et al. (2015) also indicated symmetrical dry conditions in both subtropical regions near the western Pacific during the Maunder Minimum (~1690–1740 CE) in a solar-only forcing experiment with MPI-ESM. Although Denniston et al. (2016) suggested that the Indo–Pacific tropical rain belt showed a remarkable contraction during the LIA using a volcanic-only CESM simulation, our results show that volcanic eruptions have no direct effect on centennial monsoon variations (Fig. 10B and E), which may attributed to that the effects of volcanic eruptions on monsoons maintain on interannual timescales (e.g., Anchukaitis et al., 2010; Man et al., 2014).

Nevertheless, Eroglu et al. (2016) indicated a solar-induced see-saw relationship between the EASM and ASM since the Holocene. This discrepancy could be explained as follows. During the whole Holocene, orbital parameters, such as precession, are the dominant factors to induce an opposite summer insolation between two hemispheres (Laskar et al., 2011). Under this background, solar activities further strength such opposite insolation changes, and lead to an anti-phase EASM-ASM variation (Eroglu et al., 2016). However, in the late Holocene (i.e., last millennium), insolation variation induced by solar activities was much larger than that arising from orbital change (Yan et al., 2015), and thus formed an in-phase EASM-ASM variation.

Overall, our results imply that synchronous variations of the EASM and ASM may be dominated by changes in solar irradiation. However, the response of climate changes to external forcing is weaker compared to reconstructions. Considering the ITCZ, for example, reconstructions imply a 5° southward migration of the ITCZ during the LIA (Sachs et al., 2009). However, the simulated OLR changed <0.5% between the MCA and LIA (Fig. 9A), which could not have induced such a large meridional shift of the reconstructed ITCZ. These weak climate responses in the PMIP3 last millennium experiments could be attributed to several reasons. First, reconstructions may overestimate long-term climate changes. The difference in TSI, the primary external forcing for climate change during the last millennium, is too small between the MCA and LIA. Suggested by reconstructions of the TSI (e.g., Steinhilber et al., 2009; Vieira et al., 2011), the TSI increased by only approximately 0.2 W/m<sup>2</sup> during the MCA relative to the LIA, which is not remarkable, considering the average TSI of 1365.3 W/m<sup>2</sup> during 850–1850 CE. Moreover, the inter-hemispheric temperature contrast was observed to be much smaller than that suggested by a 5° southward shift of the ITCZ (Donohoe et al., 2013). Second, although the MEM emphasizes common signals among models, it usually has a weaker internal variability than that of individual models, which is another important contributor to climate change. Finally, models tend to underestimate climate change in response to external forcings. For instance, most models have underestimated temperature anomalies in the Northern Hemisphere between the MCA and LIA (e.g., Phipps et al., 2013; Landrum et al., 2013; Fernandez-Donado et al., 2013), particularly for the warming during the MCA compared to the anomaly suggested

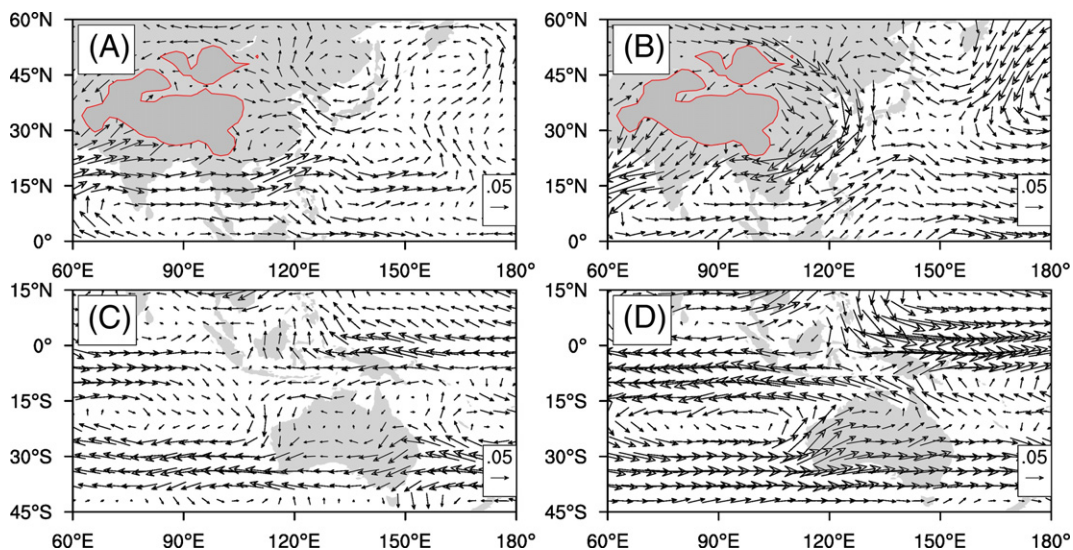
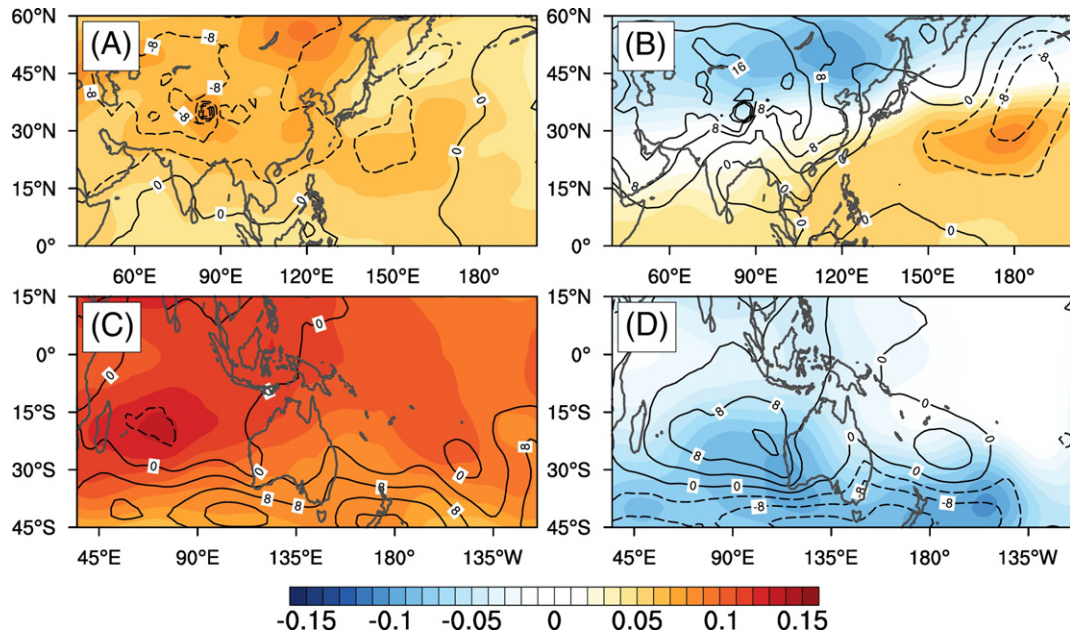


Fig. 6. Anomalies in boreal summer 850 hPa wind in the (A) MCA and (B) LIA relative to the climatological mean (850–1850 CE). (C) and (D) are the same as (A) and (B) but for austral summer. Units: m/s.



**Fig. 7.** Anomalies in boreal summer mean temperature of 500–200 hPa (color shading, units: °C) and sea level pressure (contours, unit: Pa) in the (A) MCA and (B) LIA relative to the climatological mean (850–1850 CE). (C) and (D) are the same as (A) and (B) but for austral summer.

by multiple reconstructions (e.g., Moberg et al., 2005; Mann et al., 2008). Other factors underestimated by the PMIP3 models are regional precipitation change and tropical cyclone genesis factors (e.g., Yan et al., 2016).

It should be noted that EASM and ASM variations are nonsynchronous during the MCA. Specifically, fluctuations of the EASM during the MCA conformed well to the TSI, while the weaker ASM occurring

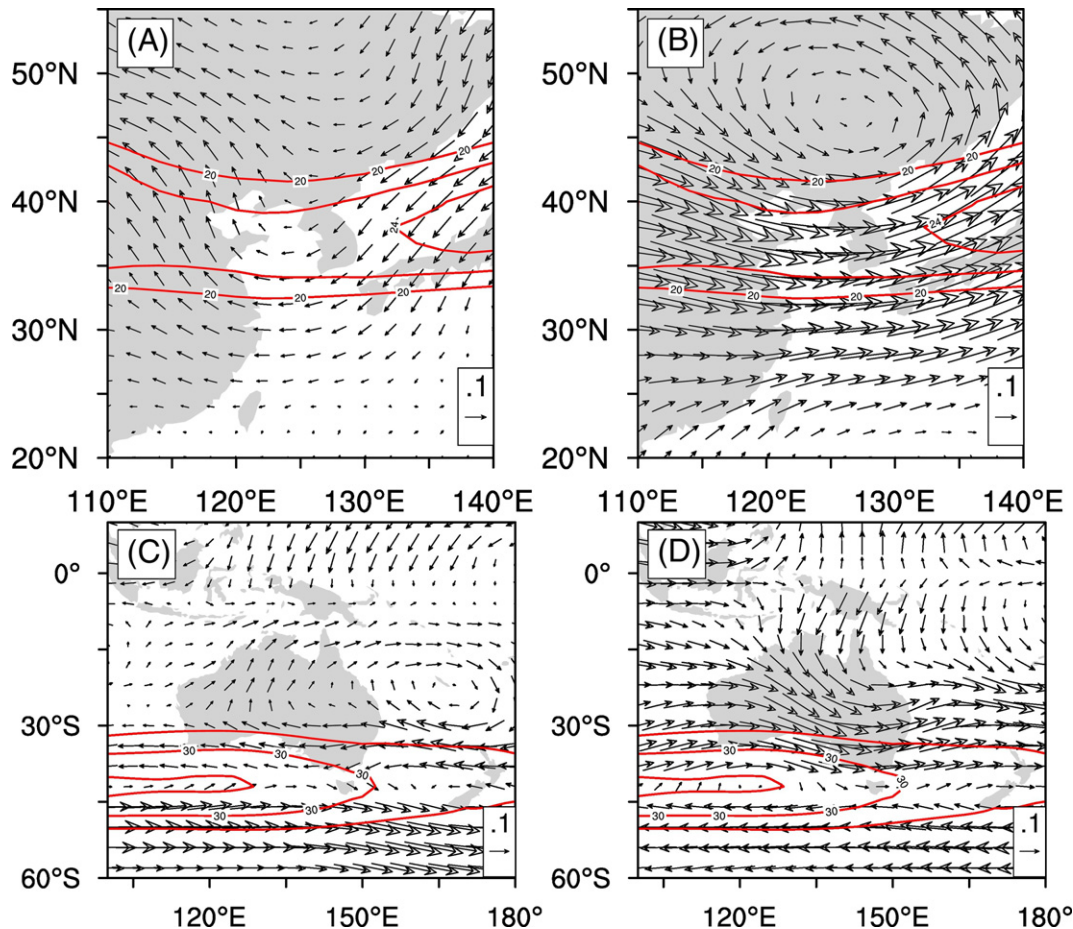


**Fig. 8.** Anomalies in boreal summer 200 hPa wind (vectors) in the (A) MCA and (B) LIA relative to the climatological mean (850–1850 CE), and the climatological mean 200 hPa zonal wind (red contours). (C) and (D) are the same as (A) and (B) but for austral summer. Units: m/s.

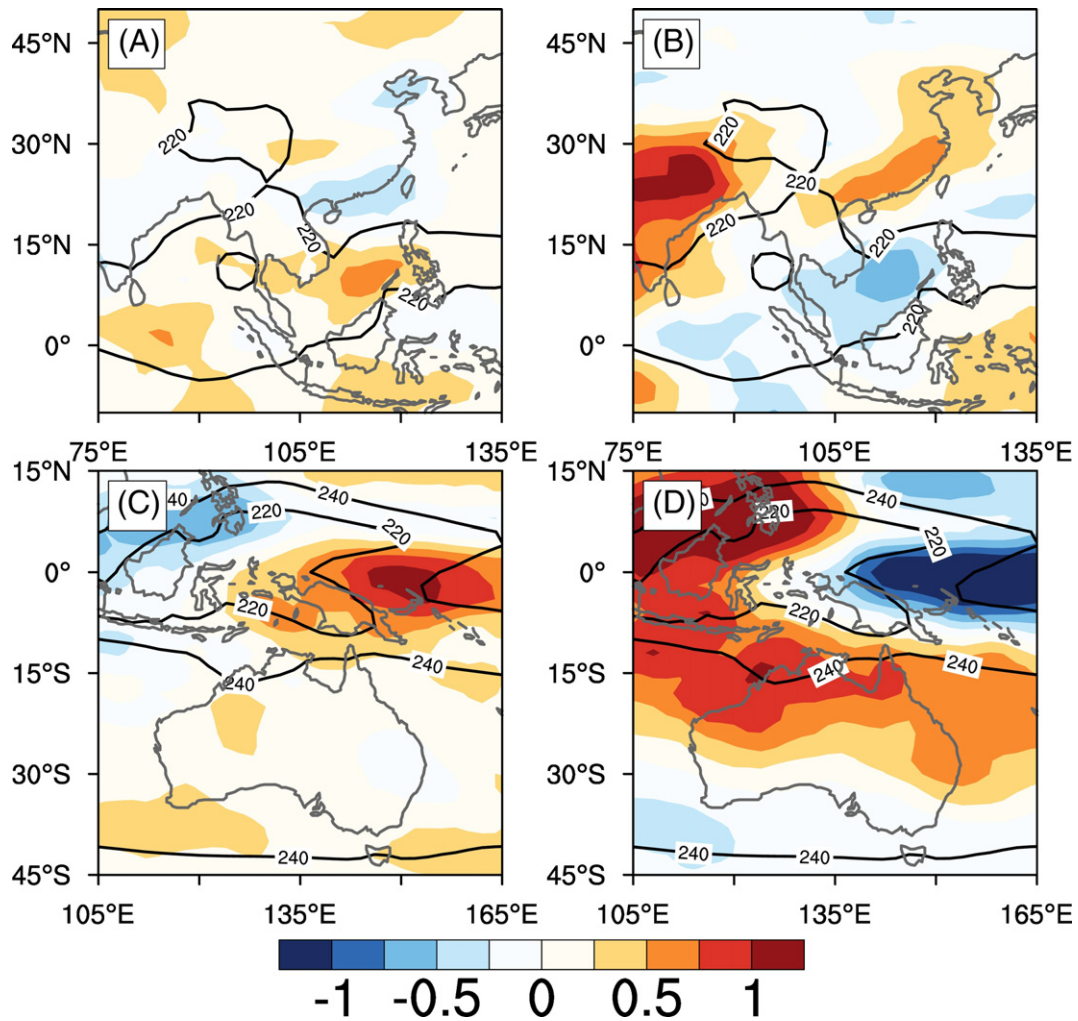


**Fig. 9.** Anomalies in boreal summer OLR field (color shading) in the (A) MCA and (B) LIA relative to the climatological mean (850–1850 CE), and the climatological mean OLR (black contours). (C) and (D) are the same as (A) and (B) but for austral summer. Units:  $W/m^2$ .

around 1100 CE correlated with a lower SST gradient. Liu et al. (2011) suggested that precipitation in extratropical regions is more sensitive to TSI than in tropical regions, which could explain the different influence of TSI on the EASM and ASM. Furthermore, the relatively weaker ASM around 1100 CE possibly resulted from the zonal position of an anomalous cyclone in the South Indian Ocean (Fig. 6C and D). Fig. 10D shows that when the South Indian Ocean warming (cooling) center was located more eastward, the ASM was stronger (weaker) than normal due to an anomalous cyclone (anticyclone) to the east.

## 6. Conclusions

The long-term variations of the EASM and ASM and their phase relationship were analyzed in this study based on PMIP3 last millennium experiments. Five models (CSIRO-Mk3L-1-2, GISS-E2-R, IPSL-CM5A-LR, MPI-ESM-P, and MRI-CGCM3) were able to reproduce the strengthened EASM and ASM during the MCA relative to the LIA. Thus, we used their ensemble mean to further explore possible dynamic mechanisms driving the reconstructed monsoon changes.

The results indicate that in the MEM simulations, EASM and ASM variations were significantly in-phase only on centennial timescales and were more synchronous during the LIA than during the MCA. The increased (decreased) EASM during the MCA (LIA) was caused by enhanced (lowered) temperature contrast between the Asian continent and adjacent oceans. This variation was also affected by the northward (southward) shift of the subtropical westerly jet and regional ITCZ over

the western Pacific region. The strengthened ASM during the MCA (LIA) was closely associated with anomalous easterly (westerly) winds from the tropical Pacific and southward (northward) migration of the ITCZ. Solar irradiation and a zonal SST gradient over the tropical Pacific region are causes of the synchronous evolution of the EASM and ASM on centennial timescales. In addition, we suggest that anomalous cyclone/anticyclone activity in the South Indian Ocean contributes to changes in the ASM.

Our conclusions are based on simulations, and thus have inevitable uncertainties. Firstly, climate models have limited skill in simulating the modern Asian–Australian monsoonal precipitation (Zhang and Moise, 2016). Secondly, whether the model sensitivity to external forcings is right remains unclear. Uncertainties also originate from the complexities of monsoon records. For example, the MCA trends of ASM were not identical even from stalagmites in the same cave (Denniston et al., 2016). Therefore, mechanisms revealed in this study require further investigation. In addition, we focus on the centennial timescale monsoon variations, while the high frequency monsoon variation is another important issue. Correlation between high frequency EASM and ASM are broadly insignificant (Fig. 4B). This result indicates that fast dynamic mechanisms for variations of the two monsoons may be different. The internal variability of climate system (e.g., ENSO) and other external forcing (e.g., volcanic eruptions) may be crucial. Thus, monsoon variations on different timescales are quite distinct and complicated, and should be addressed in a future work.

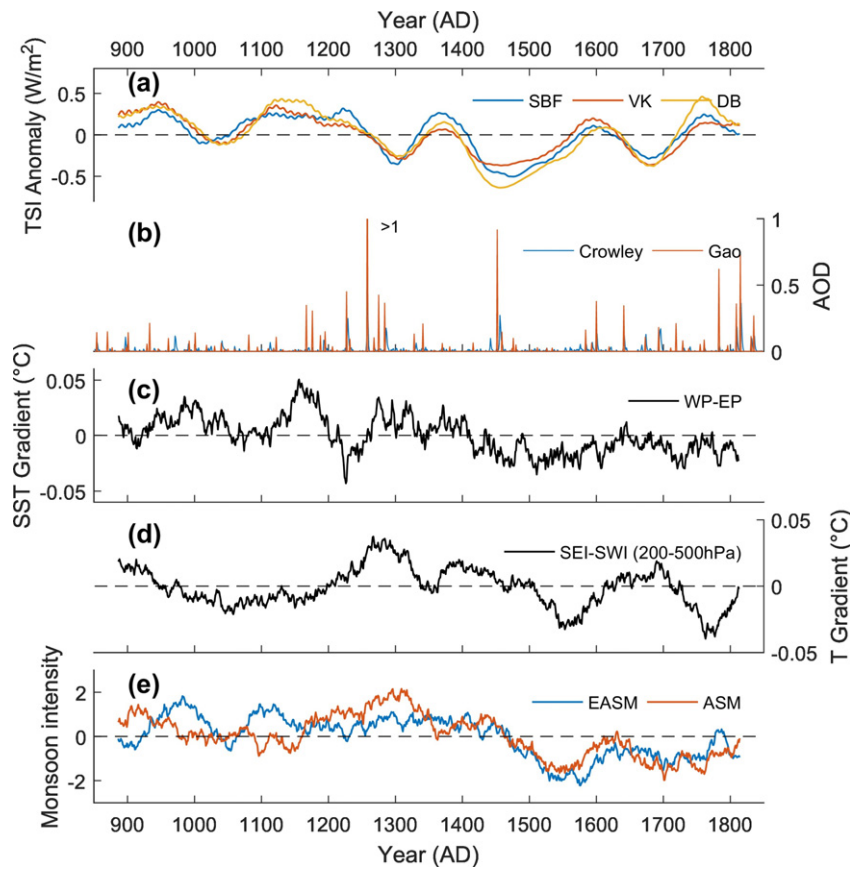


**Fig. 10.** (A) Anomalies of three TSI reconstructions (Steinhilber et al., 2009; Vieira et al., 2011; Delaygue and Bard, 2009) and (B) two volcanic reconstructions (Crowley et al., 2008; Gao et al., 2008) used in five ensemble models; (C) anomalies of annual SST gradient between the tropical western Pacific (110°–150°E, 5°S–5°N) and eastern Pacific (150°W–90°W, 5°S–5°N); (D) anomalies of troposphere temperature (500–200 hPa) difference between southeastern Indian Ocean (90°–120°E, 0–40°S) and southwestern Indian Ocean (60°–90°E, 0–40°S) in austral summer. This is an indicator of anomalous cyclone/anticyclone in the South Indian Ocean, and the cyclone (anticyclone) is located more east (west) when the index is larger; (E) the standard EASM and ASM. Anomalies are relative to the mean of 850–1850 CE. All data have smoothed by 71-a moving average, except for the volcanic reconstructions.

## Acknowledgments

We acknowledge all climate-modeling groups in the PMIP project (listed in Table 1) for producing and sharing their model output. We thank the editor and two anonymous reviewers for helpful comments on an earlier draft of this manuscript. This work was supported by the National Natural Science Foundation of China (grants number 41210007, 41402158) and Chinese Academy of Sciences–Peking University Innovation Partnership Program.

## References

- Adler, R.F., Huffman, G.J., Chang, A., Ferraro, R., Xie, P.P., Janowiak, J., Rudolf, B., Schneider, U., Curtis, S., Bolvin, D., Gruber, A., Susskind, J., Arkin, P., Nelkin, E., 2003. The version-2 global precipitation climatology project (GPCP) monthly precipitation analysis (1979–present). *J. Hydrometeorol.* 4, 1147–1167.
- An, Z.S., Wu, G.X., Li, J.P., Sun, Y.B., Liu, Y.M., Zhou, W.J., Cai, Y.J., Duan, A.M., Li, L., Mao, J.Y., Cheng, H., Shi, Z.G., Tan, L.C., Yan, H., Ao, H., Chang, H., Feng, J., 2015. Global monsoon dynamics and climate change. *Annu. Rev. Earth Planet. Sci.* 43, 29–77.
- Anchukaitis, K.J., Buckley, B.M., Cook, E.R., Cook, B.I., D'Arrigo, R.D., Ammann, C.M., 2010. Influence of volcanic eruptions on the climate of the Asian monsoon region. *Geophys. Res. Lett.* 37.
- Bothe, O., Jungclaus, J.H., Zanchettin, D., 2013. Consistency of the multi-model CMIP5/PMIP3-past1000 ensemble. *Clim. Past* 9, 2471–2487.
- Braconnot, P., Harrison, S.P., Kageyama, M., Bartlein, P.J., Masson-Delmotte, V., Abe-Ouchi, A., Otto-Bliesner, B., Zhao, Y., 2012. Evaluation of climate models using palaeoclimatic data. *Nat. Clim. Chang.* 2, 417–424.
- Burrows, M.A., Fenner, J., Haberle, S.G., 2014. Humidification in northeast Australia: dating millennial and centennial scale climate variability in the late Holocene. *Holocene* 24, 1707–1718.
- Chen, J., Chen, F., Feng, S., Huang, W., Liu, J., Zhou, A., 2015. Hydroclimatic changes in China and surroundings during the Medieval Climate Anomaly and Little Ice Age: spatial patterns and possible mechanisms. *Quat. Sci. Rev.* 107, 98–111.
- Cobb, K.M., Charles, C.D., Cheng, H., Edwards, R.L., 2003. El Niño/Southern Oscillation and tropical Pacific climate during the last millennium. *Nature* 424, 271–276.
- Conroy, J.L., Restrepo, A., Overpeck, J.T., Steinitz-Kannan, M., Cole, J.E., Bush, M.B., Colinvaux, P.A., 2009. Unprecedented recent warming of surface temperatures in the eastern tropical Pacific Ocean. *Nat. Geosci.* 2, 46–50.
- Crowley, T.J., Zielinski, G., Vinther, B., Udisti, R., Kreutz, K., Cole-Dai, J., Castellano, E., 2008. Volcanism and the little ice age. *PAGES News* 16, 22–23.
- Delaygue, G., Bard, E., 2009. Solar forcing based on Be-10 in Antarctica ice over the past millennium and beyond. *EGU General Assembly Conference Abstracts*, p. 6943.
- Denniston, R.F., Villarini, G., Gonzales, A.N., Wyrwoll, K.H., Polyak, V.J., Ummenhofer, C.C., Lachniet, M.S., Wanamaker, A.D., Humphreys, W.F., Woods, D., Cugley, J., 2015. Extreme rainfall activity in the Australian tropics reflects changes in the El Niño/Southern Oscillation over the last two millennia. *Proc. Natl. Acad. Sci. U. S. A.* 112, 4576–4581.
- Denniston, R.F., Ummenhofer, C.C., Wanamaker, A.D., Lachniet, M.S., Villarini, G., Asmerom, Y., Polyak, V.J., Passaro, K.J., Cugley, J., Woods, D., Humphreys, W.F., 2016. Expansion and contraction of the Indo-Pacific tropical rain belt over the last three millennia. *Sci. Rep.* 6, 34485.
- Ding, Y.H., Wang, Z.Y., Sun, Y., 2008. Inter-decadal variation of the summer precipitation in East China and its association with decreasing Asian summer monsoon. Part I: observed evidences. *Int. J. Climatol.* 28, 1139–1161.
- Donohoe, A., Marshall, J., Ferreira, D., Mcgee, D., 2013. The relationship between ITCZ location and cross-equatorial atmospheric heat transport: from the seasonal cycle to the Last Glacial Maximum. *J. Clim.* 26, 3597–3618.
- Eroglu, D., McRobie, F.H., Ozken, I., Stemler, T., Wyrwoll, K.H., Breitenbach, S.F.M., Marwan, N., Kurths, J., 2016. See-saw relationship of the Holocene East Asian–Australian summer monsoon. *Nat. Commun.* 7.
- Fernandez-Donado, L., Gonzalez-Rouco, J.F., Raible, C.C., Ammann, C.M., Barriopedro, D., Garcia-Bustamante, E., Jungclaus, J.H., Lorenz, S.J., Luterbacher, J., Phipps, S.J., Servonnat, J., Swingedouw, D., Tett, S.F.B., Wagner, S., Yiou, P., Zorita, E., 2013. Large-scale temperature response to external forcing in simulations and reconstructions of the last millennium. *Clim. Past* 9, 393–421.
- Gao, C.C., Robock, A., Ammann, C., 2008. Volcanic forcing of climate over the past 1500 years: an improved ice core-based index for climate models. *J. Geophys. Res. Atmos.* 113.
- Griffiths, M.L., Drysdale, R.N., Gagan, M., Zhao, J.-X., Ayliffe, L., Hellstrom, J.C., Hantoro, W., Frisia, S., Feng, Y.-X., Cartwright, I., 2009. Increasing Australian–Indonesian monsoon rainfall linked to early Holocene sea-level rise. *Nat. Geosci.* 2, 636–639.

- He, J.H., Sun, C.H., Liu, Y.Y., Matsumo, J., Li, W.J., 2007. Seasonal transition features of large-scale moisture transport in the Asian-Australian monsoon region. *Adv. Atmos. Sci.* 24, 1–14.
- Huang, R.H., Wu, Y.F., 1989. The influence of ENSO on the summer climate change in China and its mechanism. *Adv. Atmos. Sci.* 6, 21–32.
- Hu, C.Y., Henderson, G.M., Huang, J.H., Xie, S., Sun, Y., Johnson, K.R., 2008. Quantification of Holocene Asian monsoon rainfall from spatially separated cave records. *Earth Planet. Sci. Lett.* 266, 221–232.
- Jiang, D.B., Wang, H.J., 2005. Natural interdecadal weakening of East Asian summer monsoon in the late 20th century. *Chin. Sci. Bull.* 50, 1923–1929.
- Kajikawa, Y., Wang, B., Yang, J., 2010. A multi-time scale Australian monsoon index. *Int. J. Climatol.* 30, 1114–1120.
- Kutzbach, J.E., Liu, X.D., Liu, Z.Y., Chen, G.S., 2008. Simulation of the evolutionary response of global summer monsoons to orbital forcing over the past 280,000 years. *Clim. Dyn.* 30, 567–579.
- Landrum, L., Otto-Bliesner, B.L., Wahl, E.R., Conley, A., Lawrence, P.J., Rosenbloom, N., Teng, H.Y., 2013. Last millennium climate and its variability in CCSM4. *J. Clim.* 26, 1085–1111.
- Laskar, J., Fienga, A., Gastineau, M., Manche, H., 2011. La2010: a new orbital solution for the long-term motion of the Earth. *Astron. Astrophys.* 532.
- Lau, N.C., Nath, M.J., 2000. Impact of ENSO on the variability of the Asian-Australian monsoons as simulated in GCM experiments. *J. Clim.* 13, 4287–4309.
- Li, X.F., Yu, J.J., Li, Y., 2013. Recent summer rainfall increase and surface cooling over Northern Australia since the late 1970s: a response to warming in the tropical Western Pacific. *J. Clim.* 26, 7221–7239.
- Liu, J., Wang, B., Ding, Q.H., Kuang, X.Y., Soon, W.L., Zorita, E., 2009. Centennial variations of the global monsoon precipitation in the last millennium: results from ECHO-G model. *J. Clim.* 22, 2356–2371.
- Liu, J., Wang, B., Wang, H.L., Kuang, X.Y., Ti, R.Y., 2011. Forced response of the East Asian summer rainfall over the past millennium: results from a coupled model simulation. *Clim. Dyn.* 36, 323–336.
- Man, W.M., Zhou, T.J., Jungclaus, J.H., 2012. Simulation of the East Asian summer monsoon during the last millennium with the MPI Earth system model. *J. Clim.* 25, 7852–7866.
- Man, W.M., Zhou, T.J., Jungclaus, J.H., 2014. Effects of large volcanic eruptions on global summer climate and East Asian monsoon changes during the last millennium: analysis of MPI-ESM simulations. *J. Clim.* 27, 7394–7409.
- Mann, M.E., Zhang, Z., Hughes, M.K., Bradley, R.S., Miller, S.K., Rutherford, S., Ni, F., 2008. Proxy-based reconstructions of hemispheric and global surface temperature variations over the past two millennia. *Proc. Natl. Acad. Sci. U. S. A.* 105, 13252–13257.
- Meehl, G.A., Arblaster, J.M., 1998. The Asian-Australian monsoon and El Niño Southern Oscillation in the NCAR Climate System Model. *J. Clim.* 11, 1356–1385.
- Moberg, A., Sonechkin, D.M., Holmgren, K., Datsenko, N.M., Karlen, W., Lauritzen, S.E., 2005. Highly variable Northern Hemisphere temperatures reconstructed from low- and high-resolution proxy data. *Nature* 433, 613–617.
- Mohtadi, M., Prange, M., Steinke, S., 2016. Palaeoclimatic insights into forcing and response of monsoon rainfall. *Nature* 533, 191–199.
- Nicholls, N., McBride, J.L., Ormerod, R.J., 1982. On predicting the onset of the Australian wet season at Darwin. *Mon. Weather Rev.* 110, 14–17.
- Partin, J.W., Cobb, K.M., Adkins, J.F., Clark, B., Fernandez, D.P., 2007. Millennial-scale trends in west Pacific warm pool hydrology since the Last Glacial Maximum. *Nature* 449, 452–453.
- Phipps, S.J., McGregor, H.V., Gergis, J., Gallant, A.J., Neukom, R., Stevenson, S., Ackerley, D., Brown, J.R., Fischer, M.J., Van Ommen, T.D., 2013. Paleoclimate data–model comparison and the role of climate forcings over the past 1500 years. *J. Clim.* 26, 6915–6936.
- Rouillard, A., Skrzypek, G., Turney, C., Dogramaci, S., Hua, Q., Zawadzki, A., Reeves, J., Greenwood, P., O'Donnell, A.J., Grierson, P.F., 2016. Evidence for extreme floods in arid subtropical northwest Australia during the Little Ice Age chronozone (CE 1400–1850). *Quat. Sci. Rev.* 144, 107–122.
- Rustic, G.T., Koutavas, A., Marchitto, T.M., Linsley, B.K., 2015. Dynamical excitation of the tropical Pacific Ocean and ENSO variability by Little Ice Age cooling. *Science* 350, 1537–1541.
- Sachs, J.P., Sachse, D., Smittenberg, R.H., Zhang, Z., Battisti, D.S., Golubic, S., 2009. Southward movement of the Pacific intertropical convergence zone AD 1400–1850. *Nat. Geosci.* 2, 519–525.
- Sen Gupta, A., Jourdain, N.C., Brown, J.N., Monselesan, D., 2013. Climate drift in the CMIP5 models. *J. Clim.* 26, 8597–8615.
- Shi, J., Yan, Q., Jiang, D., Min, J., Jiang, Y., 2016. Precipitation variation over eastern China and arid central Asia during the past millennium and its possible mechanism: perspectives from PMIP3 experiments. *J. Geophys. Res. Atmos.* 121.
- Song, F.F., Zhou, T.J., Qian, Y., 2014. Responses of East Asian summer monsoon to natural and anthropogenic forcings in the 17 latest CMIP5 models. *Geophys. Res. Lett.* 41, 596–603.
- Steinhilber, F., Beer, J., Frohlich, C., 2009. Total solar irradiance during the Holocene. *Geophys. Res. Lett.* 36.
- Tan, M., 2007. Climatic differences and similarities between Indian and East Asian Monsoon regions of China over the last millennium: a perspective based mainly on stalagmite records. *Int. J. Speleol.* 36, 75–81.
- Tao, S.-Y., 1987. A review of recent research on the East Asian summer monsoon in China. *Review in Monsoon Meteorology*, pp. 60–92.
- Taylor, K.E., 2001. Summarizing multiple aspects of model performance in a single diagram. *J. Geophys. Res.-Atmos.* 106, 7183–7192.
- Vieira, L.E.A., Solanki, S.K., Krivova, N.A., Usoskin, I., 2011. Evolution of the solar irradiance during the Holocene. *Astron. Astrophys.* 531, A6.
- Wang, Y., Cheng, H., Edwards, R.L., He, Y., Kong, X., An, Z., Wu, J., Kelly, M.J., Dykoski, C.A., Li, X., 2005a. The Holocene Asian monsoon: links to solar changes and North Atlantic climate. *Science* 308, 854–857.
- Wang, Y.M., Lean, J.L., Sheeley, N.R., 2005b. Modeling the sun's magnetic field and irradiance since 1713. *Astrophys. J.* 625, 522–538.
- Wyrwoll, K.H., Liu, Z.Y.S., Chen, G., Kutzbach, J.E., Liu, X.D., 2007. Sensitivity of the Australian summer monsoon to tilt and precession forcing. *Quat. Sci. Rev.* 26, 3043–3057.
- Yan, H., Sun, L., Oppo, D.W., Wang, Y., Liu, Z., Xie, Z., Liu, X., Cheng, W., 2011. South China Sea hydrological changes and Pacific Walker Circulation variations over the last millennium. *Nat. Commun.* 2, 293.
- Yan, H., Wei, W., Soon, W., An, Z.S., Zhou, W.J., Liu, Z.H., Wang, Y.H., Carter, R.M., 2015. Dynamics of the intertropical convergence zone over the western Pacific during the Little Ice Age. *Nat. Geosci.* 8, 315–320.
- Yan, Q., Wei, T., Zhang, Z., 2016. Variations in large-scale tropical cyclone genesis factors over the western North Pacific in the PMIP3 last millennium simulations. *Clim. Dyn.* 1–14.
- Zhang, H., Moise, A., 2016. The Australian summer monsoon in current and future climate. *The Monsoons and Climate Change*. Springer, pp. 67–120.
- Zhang, L.X., Zhou, T.J., 2015. Drought over East Asia: a review. *J. Clim.* 28, 3375–3399.
- Zhang, Y.C., Kuang, X.Y., Guo, W.D., Zhou, T.J., 2006. Seasonal evolution of the upper-tropospheric westerly jet core over East Asia. *Geophys. Res. Lett.* 33.
- Zhang, P., Cheng, H., Edwards, R.L., Chen, F., Wang, Y., Yang, X., Liu, J., Tan, M., Wang, X., Liu, J., An, C., Dai, Z., Zhou, J., Zhang, D., Jia, J., Jin, L., Johnson, K.R., 2008. A test of climate, sun, and culture relationships from an 1810-year Chinese cave record. *Science* 322, 940–942.
- Zhou, T.J., Yu, R.C., 2005. Atmospheric water vapor transport associated with typical anomalous summer rainfall patterns in China. *J. Geophys. Res. Atmos.* 110.